Insights into Li–S Battery Cathode Capacity Fading Mechanisms: Irreversible Oxidation of Active Mass during Cycling

Article *in* Journal of The Electrochemical Society · September 2012

DOI: 10.1149/2.020211jes

4 authors:

Yan Diao

10 PUBLICATIONS **365** CITATIONS

SEE PROFILE

Kai Xie

National University of Defense Technology

64 PUBLICATIONS **931** CITATIONS

SEE PROFILE

Shizhao Xiong

National University of Defense Technology

20 PUBLICATIONS **406** CITATIONS

SEE PROFILE

Xiaobin Hong

Defence Technology Institute

22 PUBLICATIONS **571** CITATIONS

SEE PROFILE

Insights into Li-S Battery Cathode Capacity Fading Mechanisms: Irreversible Oxidation of Active Mass during Cycling

Yan Diao, Kai Xie, Shizhao Xiong and Xiaobin Hong

J. Electrochem. Soc. 2012, Volume 159, Issue 11, Pages A1816-A1821.
doi: 10.1149/2.020211jes

Journal of The Electrochemical Society, **159** (11) A1816-A1821 (2012)
0013-4651/2012/159(11)/A1816/6/$28.00 © The Electrochemical Society

Insights into Li-S Battery Cathode Capacity Fading Mechanisms: Irreversible Oxidation of Active Mass during Cycling

Yan Diao,[z] Kai Xie, Shizhao Xiong,[*] and Xiaobin Hong

College of Aerospace and Materials Engineering, National University of Defense Technology, Changsha 410073, China

The solid components deposited in sulfur cathode during cycling for Li-S battery is studied in this work. ROLi, HCO_2Li, Li_xSO_y and Li_2S (or Li_2S_2) are proved to be the main components by the methods of Fourier transform infrared (FTIR), Raman spectra and X-ray photoelectron spectroscopy (XPS). ROLi and HCO_2Li are solvent degradation products existed in electrolyte. The reversibility of Li_2S and Li_2S_2 are not serious as in previous reports. ROLi, HCO_2Li and Li_xSO_y co-deposited with Li_2S or Li_2S_2 in discharge process lead to the cathodes performance deterioration. Lithium salts such as $LiNO_3$ and LiTFSI can oxidize sulfur compounds to higher oxidation states, and Li_xSO_y species increased with cycling indicates the active mass irreversible oxidation that may be another important reason for the capacity fading of Li-S battery.
 [DOI: 10.1149/2.020211jes]

Manuscript submitted June 25, 2012; revised manuscript received July 31, 2012. Published September 5, 2012.

Rechargeable Li-S battery possesses more advantages over the conventional lithium ion battery, but the practical use faces with a variety of problems such as serious capacity fading and poor cycle performance. The most acceptable electrode reactions of the sulfur cathode include multistep redox reactions. During discharge process, elemental sulfur in solid phase $S_{8\,(s)}$ is firstly dissolved in electrolyte as $S_{8\,(l)}$, and then reduced to lithium polysulfide gradually. Intermediate products of high ordered lithium polysulfide (Li_2S_n, $3 \leq n \leq 8$) are soluble in electrolyte, but low ordered lithium polysulfide (Li_2S_2 and Li_2S) are insoluble. Different from conventional lithium ion battery, electrolyte just takes the role of Li^+ transfer medium. In Li-S system, large amount of electrochemical products dissolve in electrolyte and make it difficult to isolate lithium anode from active mass absolutely. Thus, capacity fading mechanisms of Li-S battery should be considered from different aspects.

Firstly, lithium anode reacted with high ordered lithium polysulfide (Li_2S_n, $3 \leq n \leq 8$) described as the shuttle phenomenon in electrolyte resulting in active mass diminishing. At the same time, metallic lithium reacted with solvent causing electrolyte degradation. All of these extra reactions could lead to capacity fading.[1–3] Great efforts had been made to study the electrolyte, both the organic solvent and the lithium salts how to react with lithium anode. Various inorganic and organic lithium compounds such as Li_2CO_3, Li_2O, LiOH, LiF, alkyl carbonate species ($ROCO_2Li$), alkoxy species ROLi, and alkyl carboxylate species RCOOLi were reportedly detected in lithium surface film.[4–10] Mikhaylik et al. argued that in Li-S battery the most common solvent 1,2-dimethoxyethane (DME) and 1,3-dioxolane (DOL) decomposed into lithium 2-methoxyethoxide.[11] Aurbach[12] described all the possible reduction processes and the various functional groups appearing in the lithium surface films formed in DOL/LiTFSI, Li_2S_n, and $LiNO_3$ solutions. It was proved that the formation of insoluble Li_xNO_y species and Li_xSO_y species could passivate the Li electrodes and thus prevented the continuous shuttle phenomenon.

Secondly, in sulfur cathode, researchers considered that residual irreversible Li_2S_2 and Li_2S after charging resulted in active mass loss. And the formation of insoluble Li_2S or Li_2S_2 at cracked surfaces of carbon particles caused cathode structural failure also leading to capacity fading.[3,13–15] But the irreversible degree of the Li_2S_2 and Li_2S was not quite clear. Would the electrolyte degradation affect the performance of the sulfur cathode? And except the formation of Li_2S_2 and Li_2S, whether there were any other components also deposited in cathodes. So the components of the surface layer deposited in cathodes (Fig. 2) and the formation processes should be investigated in detail.

In this work, identification the components of solid products in the very common electrolyte solutions was carried out by scanning electron microscope (SEM), Fourier transform infrared (FTIR), Raman spectra and X-ray photoelectron spectroscopy (XPS) measurements. Though $LiNO_3$ was always used as an additive to the electrolyte in Li–S battery, in order to exclude the effect of sulfur contained species in lithium salts on identifying the products, 0.5M $LiNO_3$/DOL/DME (1:1, V:V) electrolyte system was studied. Compared the results with 0.5M $LiN(SO_2CF_3)_2$ (LiTFSI)/DOL/DME electrolyte system, some important factors leading to capacity fading were suggested which had not been mentioned in previous researches.

Experimental

The electrochemical properties of products were investigated using two electrode disk cells. The sulfur cathode materials consisted of 52 wt% sulfur (99.98%, Aldrich), 35wt% Super-P carbon, and 13wt% poly (vinylidene fluoride) binder. The cathode materials were slurry-cast onto a carbon-coated aluminum current collector wtih typical active material loading of 1.0 $mg \cdot cm^{-2}$. The electrodes were dried under vacuum at 50°C for 12h. The cells were assembled in an argon-filled glove box (MIKROUNA, China) using lithium metal (100 μm, Denway, China) as anode and a porous polyolefin separator (Celgard 2500). The cells were sealed with about 0.04mL electrolyte (Novolyte, China) per milligram sulfur in an aluminum coated plastic pack under vacuum.

Discharge-charge performances of the cells at the current rate of 0.168mA $\cdot cm^{-2}$ were tested on a multi-channel battery tester (LAND CT2001A). All the tests were carried out at room temperature.

In order to study the electrochemical products changed with cycling on the sulfur cathodes, the cells were disassembled in argon-filled glove box, at the end of 1st and 20th cycle shown in figure 1. The sulfur cathodes were separated and rinsed several times with pure DOL (Novolyte, China) to remove electrolyte residue. Pieces of cathodes were all placed in an inert atmosphere during sample preparation and

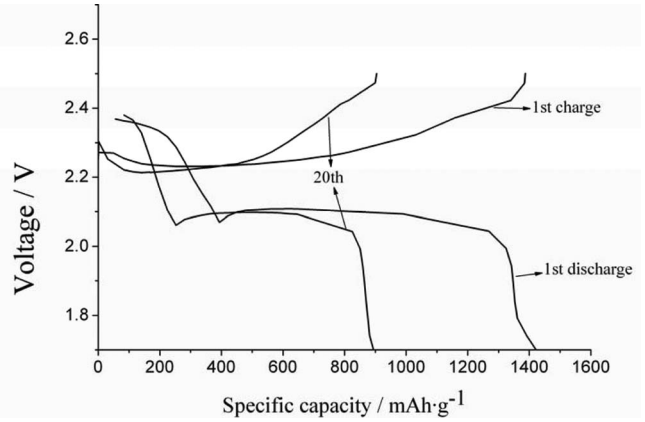

Figure 1. 20 cycles discharge-charge curves of Li-S battery.

[*]Electrochemical Society Student Member.
[z]E-mail: diaoyandiaoyan@sina.com

transformation into the tested instruments. The morphology of sulfur cathodes were obtained by scanning electron microscopy (SEM, S-4800, Hitachi). FTIR measurements were carried out on a Nicolet 6700 spectrometer. Transmission spectra were obtained with KBr pallet. Raman spectra of cathodes were detected by Bruker SENTERRA Raman spectrometer. The 532 nm line from a Krypton laser was used as an excitation sources. Spectra were obtained using 50μm × 1000μm width silt at a laser power of 20 mW. XPS measurements were carried out at a K-Alpha 1063(Thermo Fisher Scientific) spectrumeter. Monochromatic Al-Kα was used as excitation. The typical analysis area is 400 μm in diameter and the pressure for the analysis chamber is 10^{-9} mbar. Binding energy scale was corrected based on C_{1s} peak from contaminations (around 284.8 eV) as the internal binding energy standard. The Shirley background, the mixed Gaussian/Lorentzian approach, was used for the fitting of the high resolution O_{1s}, N_{1s}, C_{1s}, S_{2p}, and Li_{1s} peaks by the software (Thermo Avantage).

Results and Discussion

Analysis of solid products on cathodes in $LiNO_3$/DOL/DME electrolyte system.— The morphology of sulfur cathodes were investigated by SEM shown in Figure 2. In original cathodes (prior to discharge process), sulfur-carbon composite particles on cathode were dispersed homogeneously (Fig. 2a). At the end of discharge cycle (Fig. 2b and 2d), large amount of solid compounds were deposited on cathode, and the insoluble agglomerates accumulated on the surface made the morphology of cathodes different from the original cathode entirely.[13,14,16] At the end of charge cycle (Fig. 2c and 2e), some solid compounds were remained on cathode. Researchers considered that the residual compounds were irreversible Li_2S_2 and Li_2S, which could not contribute to discharge capacity in next cycles, causing active mass loss at the cathode side. And the formation of insoluble Li_2S or Li_2S_2 at cracked surfaces of carbon particles caused cathode structural failure also leading to capacity fading.[2] In Figure 2c and 2e, there was no powerful evidence to prove the formation of solid sulfur, S_8.

From the SEM image, it was difficult to confirm the components of sulfur cathode, and the irreversible degree of Li_2S_2 and Li_2S. In order to identify the solid compounds deposited on cathodes, FTIR and Raman spectra were used to confirm and characterize the components. Because the results of the 1st cycle and the 20th cycle were similar, only a few representative spectra of the 20th cycle were shown in Figure 3. Peak assignments for the FTIR and Raman spectra obtained in these studies were summarized in Tables I and also marked near the main peaks. In Raman spectra, the most prominent peaks of amorphous carbon were the G peak at about 1600 cm^{-1} and D peak at about 1360 cm^{-1}.[17] Compared with FTIR spectra, peaks lower than 500 cm^{-1} related to S–S bands reflected the formation of sulfur in charge cycles.[18,19] The spectra of discharged cathodes reflected the obvious formation of HCO_2Li from the peaks at 1640 cm^{-1} and 1428 cm^{-1}.[12] The characteristic peaks at 1002 cm^{-1} and 1124 cm^{-1} were related to the C–O band stretching vibration due to ROLi species. HCO_2Li and ROLi were the reduction products of electrolyte solvents. Peaks at 670 cm^{-1}, 1002 cm^{-1}, 1124 cm^{-1}, 1271cm $^{-1}$ reflected the possible species, Li_xSO_y containing S–O and S = O bonds.[18] The superposition of C–O and S–O(S=O) bands at 1002 cm^{-1} and 1124 cm^{-1} made the assignment of species containing S–O obscure, and the FTIR and Raman spectra could not provide enough information about the formation of lithium sulfides, so a semi-quantitative method XPS was used to further confirm the products.

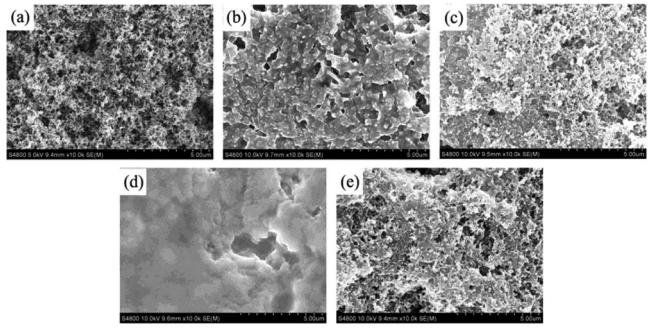

Figure 2. SEM images of the sulfur cathodes at the end of cycles. (a) the initial cathode, (b) the 1st discharge cycle, (c) the 1st charge cycle, (d) the 20th discharge cycle, (e) the 20th charge cycle.

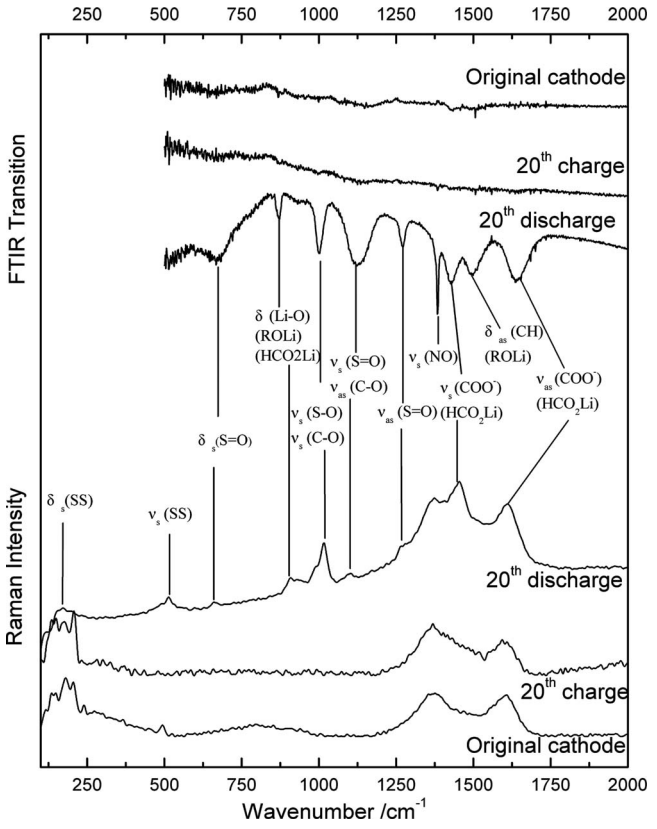

Figure 3. FTIR and Raman spectra of sulfur cathodes after cycling in 0.5M $LiNO_3$/DOL/DME solutions.

Figure 4 showed C_{1s}, O_{1s}, F_{1s}, S_{2p} and Li_{1s} spectra of sulfur cathodes after cycling. The response of N_{1s} related to both samples was close to the noise level, thereby nitrogen spectra were not presented herein. In original cathode, the C_{1s} peak at 284.8 eV attributed to C–C, and peaks located at 286.7 eV and 291.0 eV were assigned to C–H and C–F from PVdF.[10,11] At the end of discharge cycles, because of the discharge products deposition on cathodes, the C_{1s} and F_{1s} signals

Table I. Vibrational frequencies and assignments for species.

Infrared wavenumber/ cm^{-1}	Raman wavenumber/ cm^{-1}	Vibrational mode	Assignments Species
	174	δ_s(S–S)	S_2^{2-}
	514	ν_s (S–S)	S_2^{2-}
670	663	δ_s (S=O)	Sulfone, $S_2O_3^{2-}$
870	911	δ(Li-O)	HCO_2Li, ROLi
1002	1017	ν_s (C–O) ν_s (S–O)	ROLi, $S_2O_3^{2-}$
1124	1104	ν_{as} (C–O) ν_s (S=O)	ROLi, Sulfone, $S_2O_3^{2-}$
1271	1271	ν_{as} (S=O)	Sulfone, $S_2O_3^{2-}$
1385	1374	ν_s (NO)	$–NO_2$
1428	1454	ν_s (COO^-)	HCO_2Li
1490		δ_{as} (CH, CH_2, CH_3)	ROLi
1640	1609	ν_{as} (COO^-)	HCO_2Li

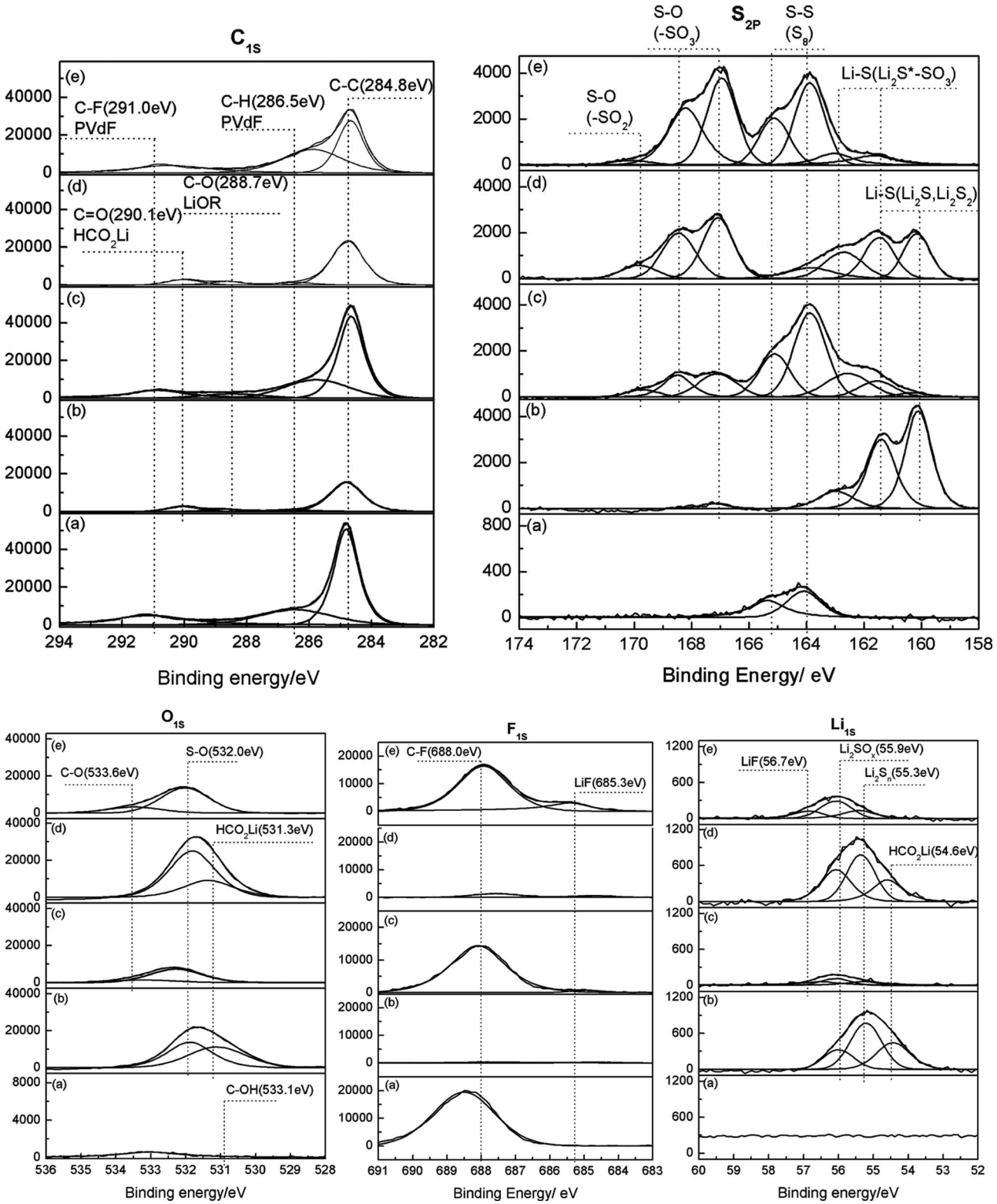

Figure 4. XPS spectra of sulfur cathodes after cycling in 0.5M $LiNO_3$/DOL/DME solutions. (a) the Original cathode; (b) Cathode of the 1st discharge cycle; (c) Cathode of the 1st charge cycle; (d) Cathode of the 20th discharge cycle; (e) Cathode of the 20th charge cycle.

from PVdF were weak. At the end of discharge cycles, the C_{1s} peak at 288.7 eV corresponding to C–O and 290.1 eV corresponding to C=O were observed. This finding confirmed the formation of ROLi and HCO_2Li.[5,7,9] The Li_{1s} peak at 56.7 eV and F_{1s} peak at 685.3 eV were assigned to LiF, which might be the production of PVdF reacted with electrolyte.[20] Li_{1s} peak at 55.3 eV was assigned to Li-S band from Li_2S or Li_2S_2.[12]

Table II showed the assignments for deconvoluted peaks in S_{2p} spectrum, and the content analysis of sulfur contained species in cathodes during cycling. S_{2p} peaks at 164.0 eV and 165.3 eV were the

Table II. Assignments for deconvoluted peaks in the S_{2p} spectrum, and the content analysis of sulfur contained species in cathodes during cycles.

Band	Binding Energy/eV	Assignments Species	Original Cathode	1st Discharge	1st Charge	20th Discharge	20th Charge
Li–S	160.0	Li_2S, Li_2S_2[12]		48.69	1.66	15.29	
	161.5	Li_2S, Li_2S_2,[12] Li_2S^*–SO_3		37.56	7.45	15.69	5.51
	162.9	Li_2S^*–SO_3[7,12,20]		11.28	13.55	12.77	4.76
S–S	164.0	S_8[21,22]	54.29		35.90	6.91	24.84
	165.3	S_8[21,22]	45.71		18.07		14.47
S–O	167.0	Li_2S–S^*O_3[7,12,20]		2.47	11.73	24.07	26.80
	168.5	Li_2S–S^*O_3[7,12,20]			8.64	19.28	21.76
	169.7	$–SO_2$[7,20]			3.01	5.98	1.87

characteristic peaks of S_8 in original cathode.[7,21,22] At the end of the 1st discharge cycle, the prominent broad S_{2p} peaks around 160–162 eV were deconvoluted to two sharper peaks at 160.0 and 161.5 eV, which could be assigned to Li_2S or Li_2S_2,[7,12] and about 97.5% sulfur in cathode was in the form of Li-S band. At the end of the 1st charge cycle, 22.7% sulfur was in Li-S band, and 54% sulfur was in S–S band. About 24% sulfur was in the form of higher oxidation states Li_xSO_y, which was corresponded with the results of FTIR and Raman spectra. After 20 cycles, the oxidation state sulfur increased to 50%. In fact, the exact identification of all these sulfur species was not very important for the present work. The importance of these surface studies laid in the oxidation trends of active mass with cycling that they reflected. At the end of 20th discharge cycle, sulfur in the form of Li-S band decreased to 43.8%, and about 6.9% sulfur was in S–S band. At the end of 20th charge cycle, only 10.3% sulfur in Li-S band was residual in cathode, which reflected the reversibility of Li_2S and Li_2S_2 was better than previous reports. It was probably that, even the cathodes structural failure leading to the insulating Li_2S or Li_2S_2 isolated from carbon particles, they could also react with high ordered lithium polysulfide in electrolyte, and thus the reversibility of Li_2S and Li_2S_2 was enhanced. Though residual Li_2S_2 and Li_2S after charging in cathode resulted in active mass loss, the good reversibility of them indicated that irreversible Li_2S_2 or Li_2S could not to be the main factor leading to cathode capacity fading.

Base on the research by Aurbach[12] and Mikhaylik,[11] electrolyte and solvent degradation resulted from reactions between the solvent and metallic lithium. These reactions generate powder and insoluble films on the lithium surface, and soluble compounds in electrolyte solution. ROLi and HCO_2Li were the components of the solvent decomposition products. Aurbach found that when $LiNO_3$ was present in electrolyte, it was probably reduced on Li to insoluble Li_xNO_y species, and could oxidize sulfides to Li_xSO_y species. The fact that these species passivated the Li electrodes explained the positive effect of $LiNO_3$ in preventing the shuttle mechanism.

However, electrolyte degradation products not only deposited on the lithium anode, but also existed in the electrolyte solution. ROLi, HCO_2Li and Li_xSO_y co-deposited with Li_2S and Li_2S_2 in cathodes during discharge process, and made the active mass isolated from the conductive structure, leading to the cathodes performance deterioration. Especially, the formation of Li_xSO_y species increasing with cycling indicated the irreversible active mass loss that might be another important reason for the capacity fading of Li-S battery, which had not been mentioned in previous researches.

Analysis of solid products on cathodes in LiTFSI/DOL/DME electrolyte system.— In 0.5M LiTFSI/DOL/DME electrolyte system without the existence of $LiNO_3$, we tested the sulfur cathodes after 20 cycles. FTIR and Raman spectra were shown in Figure 5, and XPS spectra were shown in Figure 6. DOL and DME degradation products, ROLi and HCO_2Li were formed in cathodes. At the end of 20th charge cycle, few Li_2S and Li_2S_2 were left in cathodes, which indicated the good reversibility of Li_2S and Li_2S_2. In S_{2p} spectra, peaks at 169.7 eV and 170.8 eV were the characteristic peaks of sulfone ($–SO_2$) from LiTFSI. After 20 cycles, the oxidation state sulfur species were more abundant than LiTFSI and almost had the same tendency as $LiNO_3$ electrolyte reflected the formation of Li_xSO_y species. Aurbach et al. proposed the following reaction schemes as the reductive reaction of LiTFSI in electrolyte.[7,12,23]

$$LiN(SO_2CF_3)_2 + ne^- + nLi^+ \rightarrow Li_3N + Li_2S_2O_4 + LiF + C_2F_xLi_y$$

$$LiN(SO_2CF_3)_2 + 2e^- + 2Li^+ \rightarrow Li_2NCF_3SO_2 + LiF + CF_3SO_2Li$$

$$Li_2S_2O_4 + 6e^- + 6Li^+ \rightarrow 2Li_2S + 4Li_2O$$

$$Li_2S_2O_4 + 4e^- + 4Li^+ \rightarrow Li_2SO_3 + Li_2S + Li_2O$$

The degree of LiTFSI decomposition was a key factor to the source of Li_xSO_y species in LiTFSI system. So we designed cells using lithium metal anode and sulfur free carbon cathode (Super-P). The

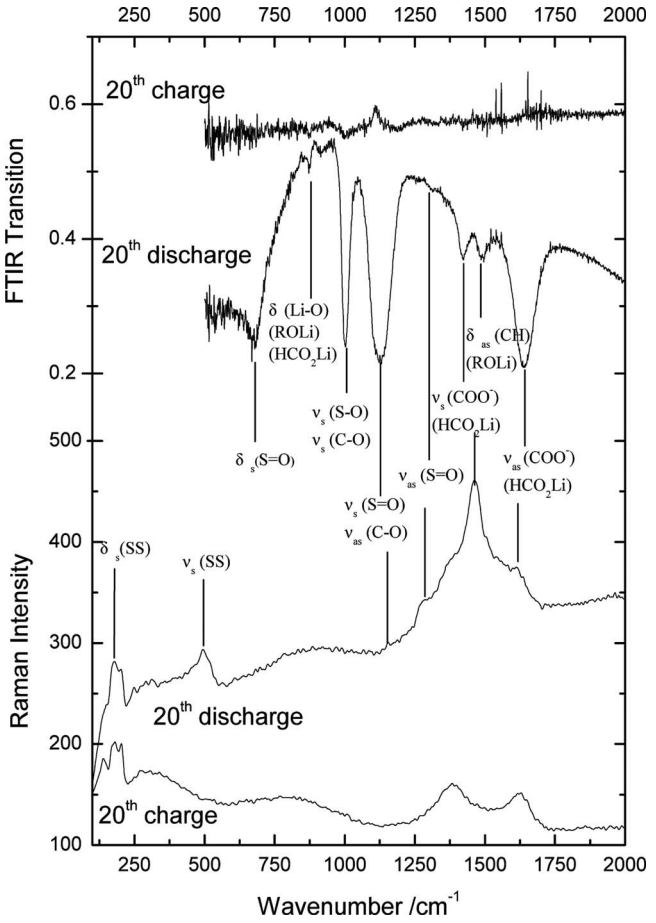

Figure 5. FTIR and Raman spectra of sulfur cathodes after cycling in 0.5M LiTFSI/DOL/DME solutions.

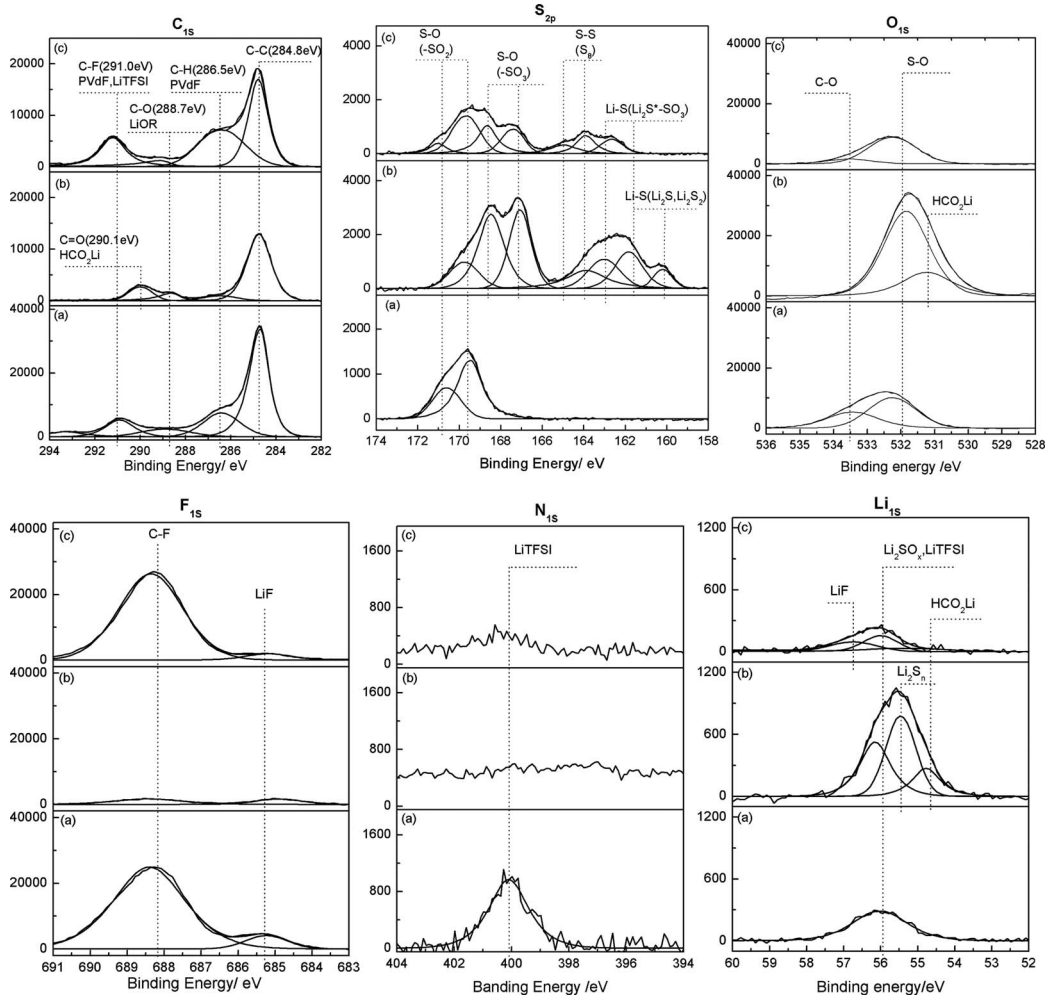

Figure 6. XPS spectra of sulfur cathodes after cycling in 0.5M LiTFSI/DOL/DME solutions. (a) LiTFSI salt; (b) Cathode of the 20th discharge cycle; (c) Cathode of the 20th charge cycle.

cells were cycled with 0.5M LiTFSI/DOL/DME electrolyte, and disassembled in argon-filled glove box after 20 cycles. After solvent of the collected electrolyte from the disassembled cell was evaporated, solid products were analyzed by XPS method. The S_{2p} and Li_{1s} spectra shown in Figure 7 confirmed that few kinds of LiTFSI decomposition species were formed and the spectra was almost the same as the spectra of LiTFSI salt. As a consequence, in LiTFSI system the Li_xSO_y species were most probably from the reaction between the LiTFSI salt and the active mass, but the reaction route should be studied in further research.

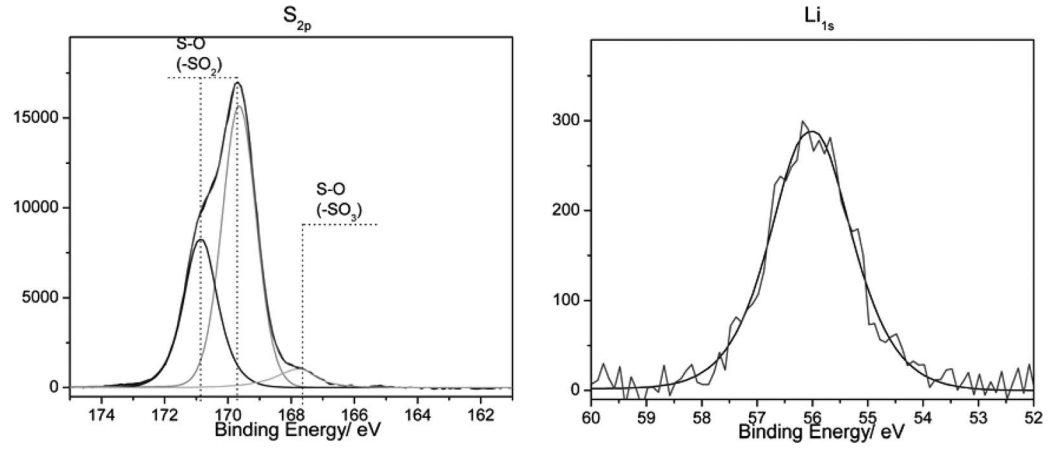

Figure 7. The S_{2p} and Li_{1s} spectra of carbon cathode after 20 cycling in 0.5M LiTFSI/DOL/DME electrolyte.

Conclusions

The reversibility of Li_2S and Li_2S_2 are not serious as in previous reports, and the irreversible Li_2S_2 or Li_2S was not the main factor leading to cathode capacity fading. Electrolyte degradation produced ROLi, HCO_2Li and Li_xSO_y in electrolyte, and they co-deposited with Li_2S and Li_2S_2 in cathodes made the cathodes performance deterioration. Lithium salts, such as $LiNO_3$ and LiTFSI, could oxidize sulfur compounds to higher oxidation states. The formation of Li_xSO_y species increased with cycling indicated the active mass irreversible oxidation that might be another important reason for the capacity fading of Li-S battery.

References

1. Y. V. Mikhaylik and J. R. Akridge, *Journal of The Electrochemical Society*, **151**, A1969 (2004).
2. X. Ji and L. F. Nazar, *Journal of Materials Chemistry*, **20**, 9821 (2010).
3. S. E. Cheon, K. S. Ko, J. H. Cho, S. W. Kim, and E. Y. Chin, *Journal of The Electrochemical Society*, **150**, A800 (2003).
4. K. Kanamura, H. Tamura, S. Shiraishi, and Z.-I. Takehara, *Electrochimica Acta*, **40**, 913 (1995).
5. A. Schechter and D. Aurbach, *Langmuir*, **15**, 3334 (1999).
6. I. Ismail, A. Noda, A. Nishimoto, and M. Watanabe, *Electrochimica Acta*, **46**, 1595 (2001).
7. H. Ota, Y. Sakata, X. Wang, J. Sasahara, and E. Yasukawa, *Journal of The Electrochemical Society*, **151**, A437 (2004).
8. S. Leroy, H. Martinez, R. Dedryve`re, D. Lemordant, and D. Gonbeau, *Applied Surface Science*, **253**, 4895 (2007).
9. D. Ensling, A. Thissen, and W. Jaegermann, *Applied Surface Science*, **255**, 2517 (2008).
10. L. Yang, T. Markmaitree, and B. L. Lucht, *Journal of Power Sources*, **196**, 2251 (2011).
11. Y. Mikhaylik, I. Kovalev, R. Schock, K. Kumaresan, J. Xu, and J. Affinito, *ECS Transactions*, **35**, 23 (2010).
12. D. Aurbach, E. Pollak, R. Elazari, and G. Salitra, *Journal of The Electrochemical Society*, **156**, A694 (2009).
13. S. E. Cheon, K. S. Ko, J. H. Cho, S. W. Kim, and E. Y. Chin, *Journal of The Electrochemical Society*, **150**, A796 (2003).
14. S. E. Cheon, S. S. Choi, J. S. Han, Y. S. Choi, B. H. Jung, and H. S. Lima, *Journal of The Electrochemical Society*, **151**, A2067 (2004).
15. Y. S. Choi, S. Kim, S. S. Choi, J. S. Han, J. D. Kim, S. E. Jeon, and B. H. Jung, *Electrochimica Acta*, **50**, 833 (2004).
16. L. Yuan, X. Qiu, L. Chen, and W. Zhu, *Journal of Power Sources*, **189**, 127 (2009).
17. H. Wang and K. Xie, *Electrochimica Acta*, **64**, 29 (2012).
18. S. A. Khan, R. W. Hughes, and P. A. Reynolds, *Vib. Spectrosc.*, **56**, 241 (2011).
19. L. Rintoul, K. Crawford, H. FShurvell, and P. M. Fredericks, *Vib. Spectrosc.*, **15**, 171 (1997).
20. C. D. Wagner, A. V. Naumkin, A. Kraut-Vass, J. W. Allison, C. J. Powell, and J. R. Rumble, NIST X-Ray Photoelectron Spectroscopy Database, NIST Standard Reference Database 20, Version 3.5., http://srdata.nist.gov/xps/ (2007).
21. Y. Yang, G. Yu, J. J. Cha, H. Wu, M. Vosgueritchian, Y. Yao, Z. Bao, and Y. Cui, *acsnano*, **5**, 9187 (2011).
22. R. Demir-Cakan, M. Morcrette, F. Nouar, C. Davoisne, T. Devic, D. Gonbeau, R. Dominko, C. Serre, and J.-M. Tarascon, *J. Am. Chem. Soc.*, **133**, 16154 (2011).
23. D. Aurbach, A. Zaban, Y. Ein-Eli, I. Weissman, O. Chusid, B. Markovsky, M. Levi, E. Levi, A. Schechter, and E. Granot, *Journal of Power Sources*, **68**, 463 (1997).